Physics and Chemistry of Minerals (2024) 51:33
https://doi.org/10.1007/s00269-024-01286-5

ORIGINAL PAPER

The thermal expansion of Ti-substituted $CaAl_{12}O_{19}$

Paul F. Schofield[1] · Andrew J. Berry[1,2] · Patricia M. Doyle[1,3,6] · Kevin S. Knight[1,4,5]

Received: 16 March 2024 / Accepted: 12 June 2024 / Published online: 5 August 2024
© The Author(s) 2024

Abstract

$CaAl_{12}O_{19}$, which can incorporate Ti as both Ti^{3+} and Ti^{4+} (charge coupled substitution with Mg^{2+}), is one of the first minerals to condense from a gas of solar composition and is used as a ceramic. It is variously known as hibonite, calcium hexaluminate ($CaO.6Al_2O_3$), and CA_6. The lattice parameters and unit cell volumes of Ti-substituted hibonite ($P6_3/mmc$) with the formulae $CaAl_{11.8}Ti^{3+}_{0.2}O_{19}$ and $CaAl_{9.8}Ti^{3+}_{0.54}Mg_{0.83}Ti^{4+}_{0.83}O_{19}$ were determined as a function of temperature from ~ 10 to 275 K by neutron powder diffraction. The thermal expansion is highly anisotropic with the expansion in c a factor of ~ 5 greater than that in a. The change in a is approximately equal for the two compounds whereas the change in c is almost 50% larger for $CaAl_{11.8}Ti^{3+}_{0.2}O_{19}$. $CaAl_{11.8}Ti^{3+}_{0.2}O_{19}$ also exhibits negative thermal expansion between 10 and 70 K. The change in unit cell volume with temperature of both compositions is well described by a two term Einstein expression. The large change in c is consistent with substitution of Ti onto the M2 and M4 sites of the R-block structural unit.

Keywords Hibonite · CA_6 · Calcium hexaluminate · Negative thermal expansion · Neutron powder diffraction · Ti^{3+}

Introduction

$CaAl_{12}O_{19}$ is known as hibonite when naturally occurring and as calcium hexaluminate ($CaO.6Al_2O_3$ or CA_6) in the ceramics industry, where it is used in composite materials (e.g. Salomao et al. 2016). Hibonite can contain Ti as both Ti^{3+}, which substitutes for Al^{3+}, and Ti^{4+}, which undergoes a charge coupled substitution with Mg^{2+} ($Ti^{4+} + Mg^{2+} = 2Al^{3+}$). A general formula for Ti-bearing hibonite is $CaAl_{12-2x-y}Mg_xTi^{4+}_xTi^{3+}_yO_{19}$. Hibonite is thought to have been the second mineral to condense from the Solar nebula and the ratio of Ti^{3+} to Ti^{4+}, expressed as $Ti^{3+}/\Sigma Ti$ where $\Sigma Ti = Ti^{3+} + Ti^{4+}$, may record the oxygen fugacity of the nebular gas (Ihinger and Stolper 1986; Beckett et al. 1988; Doyle et al. 2016; Berry et al. 2017; Zanetta et al. 2023).

Hibonite is hexagonal ($P6_3/mmc$, Z = 2) and has the magnetoplumbite structure (Utsunomiya et al. 1988; Hofmeister et al. 2004). There are five Al sites (M1-M5) and their coordination numbers and multiplicity are given by $^{[12]}Ca^{[6]}M1^{[5]}M2^{[4]}M3_2^{[6]}M4_2^{[6]}M5_6O_{19}$ (where coordination numbers are superscripted in square brackets and the multiplicity of the site is subscripted). The structure is shown in Fig. 1 and can be described in terms of polyhedral layers, called the R- and S-blocks, perpendicular to c. The R-block contains the Ca, M2 and M4 sites, while the S-block contains the M1, M3 and M5 sites. The unit cell is formed by stacking the R- and S-blocks along c in the order RSR'S', where R' and S' are rotated 180° about c relative to R and S (Bermanec et al. 1996). Ti^{3+} occupies adjacent face-sharing octahedral M4 sites, Ti^{4+} occupies both the trigonal bipyramidal M2 and M4 sites, and Mg occupies the tetrahedral M3 site (Doyle et al. 2014; Giannini et al. 2014). Ti occupancy of neighbouring M4 sites is stabilised by Ti–Ti interactions (Doyle et al. 2014).

How a material responds structurally to changes in temperature affects its bulk properties and hence use in applications. Most structures expand when heated (positive

✉ Andrew J. Berry
Andrew.Berry@anu.edu.au

1 Mineral Sciences Group, Natural History Museum, London SW7 5BD, UK

2 Research School of Earth Sciences, Australian National University, ACT, Canberra 2601, Australia

3 Department of Earth Science and Engineering, Imperial College London, London SW7 2AZ, UK

4 ISIS Science Division, Rutherford Appleton Laboratory, Didcot OX11 0QX, UK

5 School of Chemistry, University of Edinburgh, Edinburgh EH9 3FJ, UK

6 Present Address: Department of Geological Sciences, University of Cape Town, Rondebosch 7701, South Africa

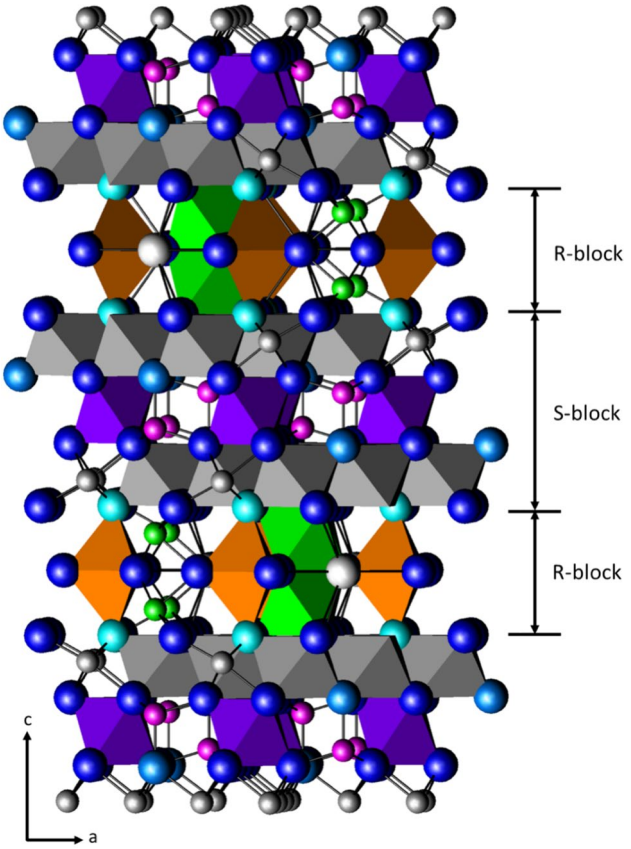

Fig. 1 The crystal structure of $CaAl_{12}O_{19}$ hibonite, with the *c*-axis vertical, shown as a composite ball-and-stick and polyhedral representation. The structural units called the R- and S-blocks are indicated. The R-block comprises the Ca site, trigonal bypyramidal M2 site and the octahedra face-sharing M4 site. The S-block comprises layers of M5 octahedra either side of a layer containing M3 tetrahedra and M1 octahedra. M1 polyhedra purple, M2 polyhedra orange, M3 atoms pink, M4 polyhedra and atoms green, M5 polyhedra and atoms grey; Ca atoms white; O1 light blue, O2 mid blue, O3, O4 and O5 dark blue

thermal expansion), but some may contract (negative thermal expansion), and others may show little or no change. Materials with small coefficients of thermal expansion are better able to withstand thermal shock and have potential uses in ceramics. A compound with negative thermal expansion can be used as a component in a composite material to give a net thermal expansion of zero, or one that can be tuned to a desired value (e.g. Evans 1998a). Thermal expansion as an intrinsic property depends on how the unit cell parameters and hence volume changes with temperature. Unit cell parameters can be determined by the refinement of diffraction data but as only peak positions rather than intensities are required the data do not need to be as good as those needed for a full structural refinement. As a result suitable patterns can be recorded quickly, enabling data to be acquired at multiple temperatures. As an example, ZrW_2O_4 (and HfW_2O_4) is a cubic material that exhibits isotropic negative thermal expansion from below 2 K to 1050 K (where it decomposes) (Mary et al. 1996). More usually, negative expansion may occur in one crystallographic direction and positive expansion in another, which together may result in a negative or positive change in volume with temperature. Compounds where this behaviour is observed over their entire stability range include $Sc_2(WO_4)_3$ (Evans et al. 1998b), $Zn_3(PO_4)_2{\cdot}4D_2O$ (Schofield et al. 2007), $Ag_3[Co(CN)_6]$ (Goodwin et al. 2008), and $MgSO_4.4DH_2O$ (Meusburger et al. 2021). Other compounds exhibit both negative and positive thermal expansion over different ranges (e.g. $LiAlSi_4O_{10}$, Knight 2014; β-SiO_2, Welche et al. 1998; $CaSO_4.2D_2O$, Schofield et al. 1996). The relative rate at which a material expands with increasing temperature is given by α, which is typically between 0 and 20×10^{-6} K^{-1}, although values > 100 are known (termed "colossal"; Goodwin et al. 2008).

The thermal expansion of a natural hibonite with the simplified composition $CaAl_{11}Mg_{0.5}Ti^{4+}{}_{0.5}O_{19}$ has been determined between 100 and 923 K by single crystal X-ray diffraction (Nagashima et al. 2010) but there are no data for hibonite containing Ti^{3+} or at low temperatures. The heat capacity of $CaAl_{12}O_{19}$ has been predicted by Hofmeister (2004). Here we investigate the thermal expansion of Ti^{3+}-substituted hibonites with the stoichiometry $CaAl_{11.8}Ti^{3+}{}_{0.2}O_{19}$ and $CaAl_{9.8}Ti^{3+}{}_{0.54}Mg_{0.83}Ti^{4+}{}_{0.83}O_{19}$, for which the structure and site occupancies have been determined previously by neutron powder diffraction (Doyle et al. 2014).

Methods

Samples were prepared with the simplified stoichiometry $CaAl_{11.8}Ti^{3+}{}_{0.2}O_{19}(Ti^{3+}/\Sigma Ti = 1.0)$ and $CaAl_{9.8}Ti^{3+}{}_{0.54}Mg_{0.83}Ti^{4+}{}_{0.83}O_{19}$ $(Ti^{3+}/\Sigma Ti = 0.4)$ by heating mixtures of $CaCO_3$, Al_2O_3, TiO_2, and MgO as pellets in a graphite crucible and atmosphere of CO at 1400 ˚C. Full experimental details are given in Doyle et al. (2014), where the samples are described by the nomenclature (Ti pfu, $Ti^{3+}/\Sigma Ti$), corresponding to (0.20, 1) and (1.37, 0.39) for the samples discussed here.

Neutron time-of-flight (TOF) powder diffraction data were recorded for each sample using the high-resolution powder diffractometer HRPD (Ibberson et al. 1992; Ibberson 2009) at the ISIS neutron spallation source, Rutherford Appleton Laboratory, UK. Samples were packed into the Al sample block of a continuous cycle cryostat and cooled to ~ 10 K. Neutron diffraction data were collected from ~ 10 to 275 K in 5 K steps (with an equilibration time at each temperature of 5 min) for a total beam exposure of 9 μAhours over a TOF range of 32–126 ms (corresponding to

d-spacings of 0.663–2.610 Å) using a backscatter detector bank at 168°. Data were binned for $\Delta t/t = 0.0003$ ms, background subtracted, normalised and corrected for absorption.

Lattice parameters were determined from whole pattern profile fitting of the diffraction data within the General Structure Analysis System (GSAS) code of Larson and Von Dreele (2004) interfaced with EXPGUI (Toby 2001). The unit cell, background (five term shifted Chebyschev function) and peak shape were refined using the model dependent Le Bail method with the initial model for each sample based on the structures reported in Doyle et al. (2014). The results for a given temperature were used as the starting parameters for the refinement of the data at the next temperature.

Results

A typical diffraction dataset and refinement are shown in Fig. 2 for $CaAl_{11.8}Ti^{3+}{}_{0.2}O_{19}$ at 8 K. The data are sufficient for accurately determining lattice parameters but not for detailed structural refinement. This is due to the short acquisition time that allowed multiple temperature steps. Data obtained with a longer acquisition time, at a single temperature, were used for structural refinement and are reported in Doyle et al. 2014. Changes in the unit cell of the samples with temperature are evident from shifts in the diffraction peaks, as shown in Fig. 3. The unit-cell parameters and hence volumes determined from the refinements, and the goodness of fit parameters, at each temperature are given in Tables S1 and S2. The changes in lattice parameters and volumes as a function of temperature are shown in Fig. 4.

The unit cell parameters of both $CaAl_{11.8}Ti_{0.2}O_{19}$ and $CaAl_{9.8}Ti^{3+}{}_{0.54}Mg_{0.83}Ti^{4+}{}_{0.83}O_{19}$ generally increase with increasing temperature, with the change in c being significantly larger than that of a (0.022 Å compared to 0.003 Å for $CaAl_{11.8}Ti_{0.2}O_{19}$ between ~10 and 275 K; Fig. 4a, b). While the change in a for the two compounds is similar the change in c for $CaAl_{11.8}Ti_{0.2}O_{19}$ is almost 50% larger.

The thermal expansion of c in $CaAl_{11.8}Ti_{0.2}O_{19}$ is negative up to ~ 70 K. The change is small (~ 0.001 Å) but clearly defined (Figs. 3, 4a). A decrease in the volume of the unit cell is not seen over this range (Fig. 4c) since the decrease in c is countered by an increase in a, resulting in an almost constant volume. Negative thermal expansion was not observed for $CaAl_{9.8}Ti^{3+}{}_{0.54}Mg_{0.83}Ti^{4+}{}_{0.83}O_{19}$.

Discussion

The thermal expansion of materials can be described empirically (e.g. Hazen and Prewitt 1977) or by a theoretical model (e.g. Knight 1996; Knight et al. 1999; Knight and Price 2008). The latter approach is based on the assumption that the specific heat capacity can be described by an Einstein model such that the variation of the unit cell as a function of temperature can be modelled by the expression (Knight 1996; Schofield et al. 1996):

$$X(\mathrm{T}) = X_0 + \frac{K}{\mathrm{e}^{\nu_E/\mathrm{T}} - 1} \quad (1)$$

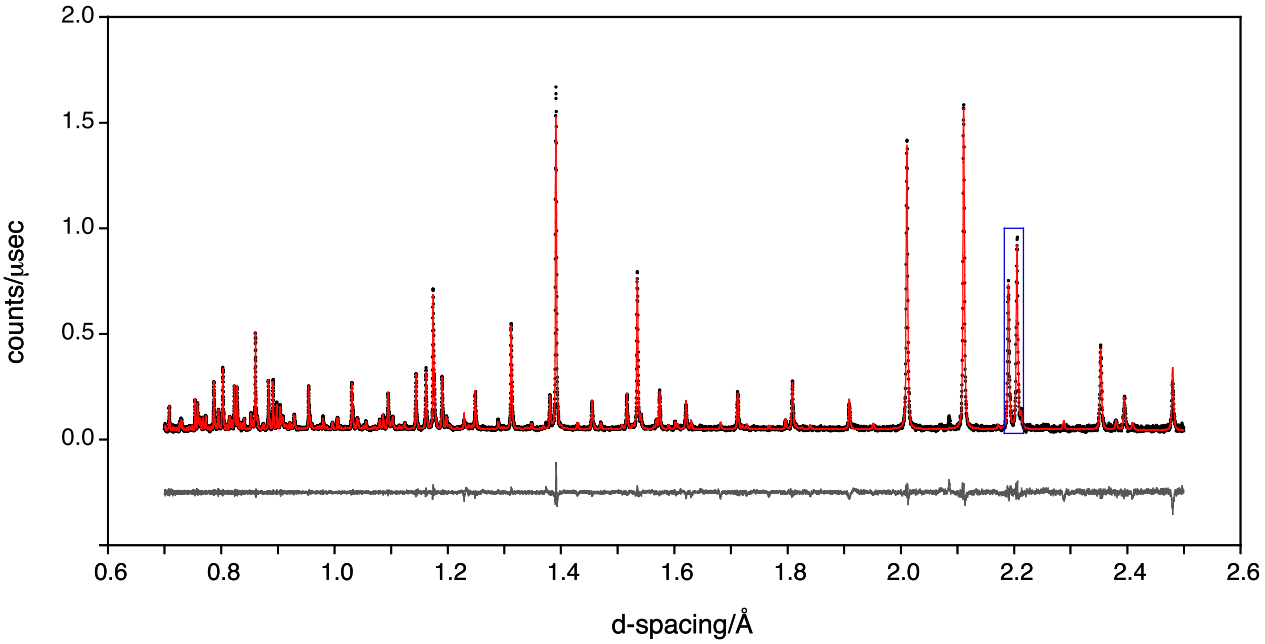

Fig. 2 Model dependent Le Bail fit (red) to the neutron powder diffraction pattern (black symbols) between 0.7 and 2.5 Å of $CaAl_{11.8}Ti_{0.2}O_{19}$ at 8 K (difference in grey). The blue box corresponds to the region shown in Fig. 3

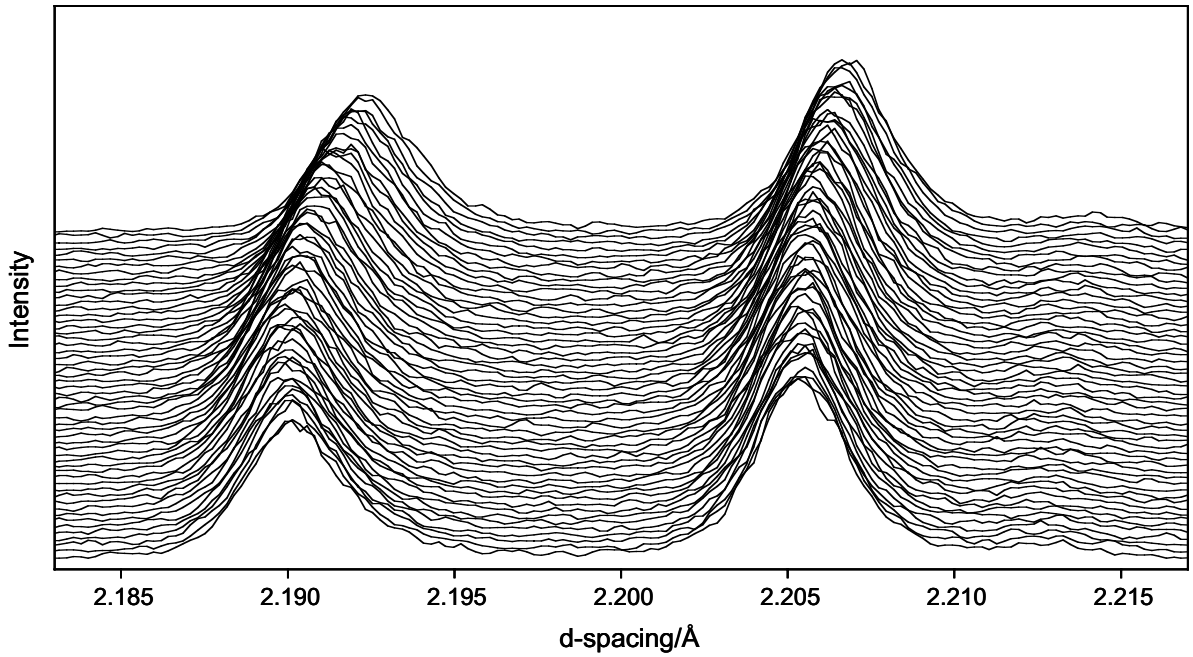

Fig. 3 Diffraction patterns between 2.183 and 2.217 Å as a function of temperature from 8 to 275 K (8 K at the bottom) for $CaAl_{11.8}Ti_{0.2}O_{19}$. The peak at ~ 2.19 Å corresponds to 0010 and that at ~ 2.205 to 204. The shift in the 0010 peak as a function of temperature shows the negative thermal expansion along the c-axis between 8 and ~ 70 K and positive thermal expansion between ~ 70 and 275 K

where X is the unit cell parameter, T the temperature in K, X_0 the unit cell parameter at 0 K, K the Einstein constant, and ν_E the effective Einstein temperature. To precisely fit the data in Tables S1 and S2, particularly at low temperatures, a two-term Einstein expression (Knight 2014) of the from:

$$X(\mathrm{T}) = X_0 + \frac{K_1}{e^{\nu_{E_1}/\mathrm{T}} - 1} + \frac{K_2}{e^{\nu_{E_2}/\mathrm{T}} - 1} \tag{2}$$

was required, whereby $K_1 < 0$ and $K_2 > 0$ can model a change from negative to positive thermal expansion. The fits to the data are shown in Fig. 4 and the resulting parameters are given in Table 1.

The isobaric thermal expansion coefficient of the unit cell parameter, $\alpha(X)$, is given by:

$$\alpha(X) = \frac{1}{X_0} \times \left[\frac{K_1 \nu_{E_1}}{\mathrm{T}^2} \times \left(\frac{e^{\nu_{E_1}/\mathrm{T}}}{\left(e^{\nu_{E_1}/\mathrm{T}} - 1\right)^2} \right) + \frac{K_2 \nu_{E_2}}{\mathrm{T}^2} \times \left(\frac{e^{\nu_{E_2}/\mathrm{T}}}{\left(e^{\nu_{E_2}/\mathrm{T}} - 1\right)^2} \right) \right] \tag{3}$$

The thermal expansion coefficients $\alpha(a)$, $\alpha(c)$ and $\alpha(\mathrm{V})$ at 275 K were calculated to be $4.2(2) \times 10^{-6}$, $7.9(2) \times 10^{-6}$, and $16.7(4) \times 10^{-6}$, respectively, for $CaAl_{11.8}Ti^{3+}{}_{0.2}O_{19}$ and $5.1(9) \times 10^{-6}$, $5.9(7) \times 10^{-6}$, and $16.1(7) \times 10^{-6}$, respectively, for $CaAl_{9.8}Ti^{3+}{}_{0.54}Mg_{0.83}Ti^{4+}{}_{0.83}O_{19}$. The temperature dependence of these coefficients is shown in Fig. 5.

Alternatively, assuming that $e^{\nu_E/\mathrm{T}} \approx (1 + \nu_E/\mathrm{T})$ at high temperatures (Schofield et al. 1996), Eq. (3) can be simplified to:

$$\alpha(X) = \frac{K_1}{X_0 \nu_{E_1}} \left(1 + \frac{\nu_{E_1}}{\mathrm{T}}\right) + \frac{K_2}{X_0 \nu_{E_2}} \left(1 + \frac{\nu_{E_2}}{\mathrm{T}}\right) \tag{4}$$

and thus the high temperature limits of $\alpha(a) = 6.6(2) \times 10^{-6}$, $\alpha(c) = 10.0(1) \times 10^{-6}$ and $\alpha(\mathrm{V}) = 25.0(4) \times 10^{-6}$ for $CaAl_{11.8}Ti^{3+}{}_{0.2}O_{19}$, and $\alpha(a) = 8.9(4) \times 10^{-6}$, $\alpha(c) = 10.2(6) \times 10^{-6}$ and $\alpha(\mathrm{V}) = 27.3(5) \times 10^{-6}$ for $CaAl_{9.8}Ti^{3+}{}_{0.54}Mg_{0.83}Ti^{4+}{}_{0.83}O_{19}$.

The thermal expansion of the c lattice parameter is significantly larger than that of a. Further, while the change in a is similar for both compounds the change in c is larger for $CaAl_{11.8}Ti^{3+}{}_{0.2}O_{19}$ than for the mixed valent sample (Fig. 4a, b). To understand these differences it is useful to consider the R- and S-block description of the structure (Fig. 1). The R-block includes the M2 and M4 sites onto which Ti substitutes. The thickness of the R-block corresponds to the distance between the apical oxygens (O1) of the trigonal bipyramidal M2 site, where O1-M2-O1 is parallel to c, while the vector between the face-sharing pairs of octahedral M4 sites is also parallel to c. Differences in the Ti occupancy of the M2 and M4 sites between the two samples will therefore produce differences in c. The mean expansion coefficient determined for a Ti^{4+}-substituted M4 site is larger than that predicted for Al occupancy (Nagashima et al. 2010). Ca, which also resides in the R-block, is under-bonded and "rattles" in its site, as a result of which the Ca-O bond expansion is only about half of that predicted (Nagashima et al. 2010).

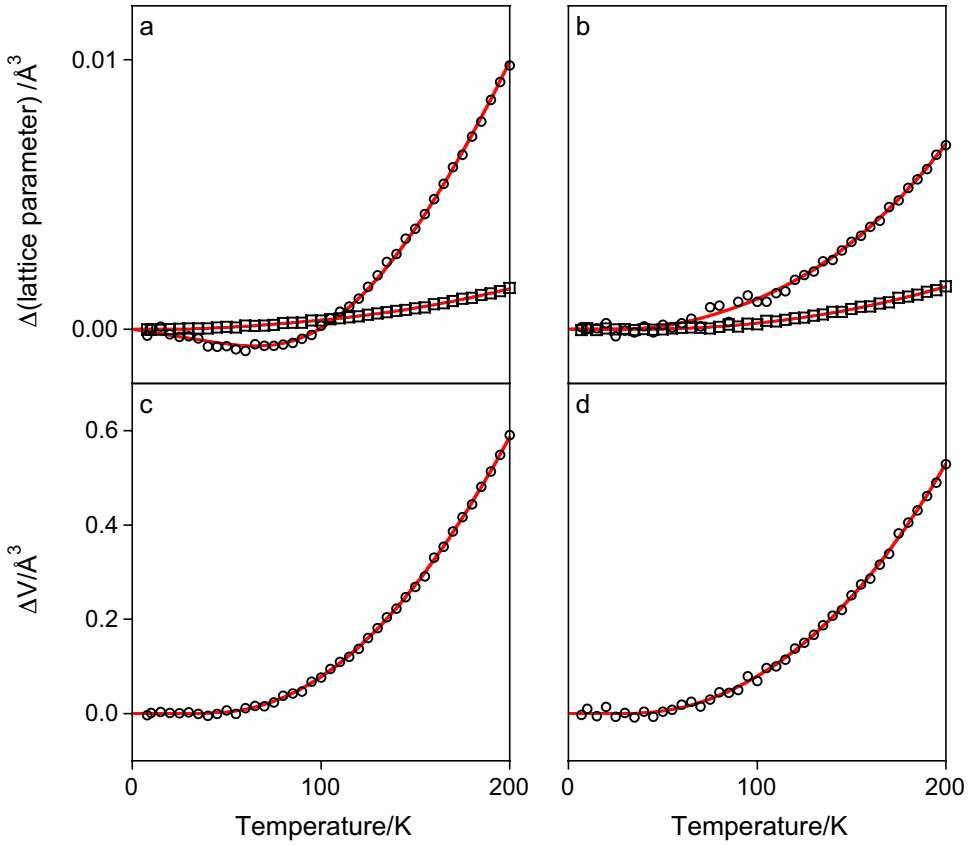

Fig. 4 Change in the *a* (squares) and *c* (circles) lattice parameters of **a** $CaAl_{11.8}Ti^{3+}_{0.2}O_{19}$, and **b** $CaAl_{9.8}Ti^{3+}_{0.54}Mg_{0.83}Ti^{4+}_{0.83}O_{19}$, and change in the unit cell volume (circles) of **c** $CaAl_{11.8}Ti_{0.2}O_{19}$, and **d** $CaAl_{9.8}Ti^{3+}_{0.54}Mg_{0.83}Ti^{4+}_{0.83}O_{19}$, as a function of temperature. The fits to the data using Eq. (2) are shown in red. A reduced temperature range is shown to highlight the agreement between the data and fit for negative expansion. Errors are smaller than the size of the symbols

Table 1 The unit cell parameter (*a*, *c*) or volume (V) at 0 K (X_0), the Einstein constant (K), and the effective Einstein temperature (ν_E) obtained by fitting the data in Tables S1 and S2 to Eq. (2)

	$CaAl_{11.8}Ti_{0.2}O_{19}$			$CaAl_{9.8}Ti^{3+}_{0.54}Mg_{0.83}Ti^{4+}_{0.83}O_{19}$		
	a	*c*	V	*a*	*c*	V
X_0	5.56305 (6)	21.89661 (2)	586.8544 (8)	5.624430 (5)	22.10064 (3)	605.469 (1)
K_1	0.00087 (4)	$-1.190\ (9)\times10^{-5}$	1.54 (2)	0.0039 (1)	0.0075 (4)	0.93 (2)
ν_{E_1}	130 (5)	1.062 (9)	308 (2)	291 (5)	207 (8)	258 (4)
K_2	0.0223 (8)	0.103 (1)	7.4 (2)	0.032 (2)	0.15 (1)	10.6 (4)
ν_{E_2}	744 (8)	450 (3)	765 (6)	875 (19)	806 (18)	824 (10)

In the S-block, only the M3-O2 bond of the tetrahedral M3 site is parallel to *c*. Incorporation of Mg on this site causes the M3-O2 bond to lengthen (Doyle et al. 2014) resulting in an increase in the thickness of the S-block. The presence of Mg on M3 is thus likely to affect the thermal expansion of the S-block, although the expansion coefficient of Mg-substituted M3 is smaller than that of Ti^{4+}-substituted M4 (Nagashima et al. 2010), and hence changes in the R-block will dominate the expansion along *c*. We note that Ti substituted Ba hexaferrite, which also has the magnetoplumbite structural type, shows larger expansion along *c* than *a* (Hernandez-Gomez et al. 2000), consistent with that found here.

The thermal expansion of the $CaAl_{11.8}Ti^{3+}_{0.2}O_{19}$ lattice parameters is controlled by the $CaAl_{12}O_{19}$ "base" structure and by the presence of Ti^{3+} on the M4 site. For the mixed-valent sample the presence of Ti^{4+} on both the M2 and M4 sites, and Mg on M3, must also be considered. The presence of 0.2 Ti^{3+} per formula unit (pfu) causes a greater expansion in *c* than the addition of 0.54 Ti^{3+} pfu plus 0.83 Ti^{4+} pfu and 0.83 Mg pfu. The fact that the mixed valent sample contains more Ti^{3+} than $CaAl_{11.8}Ti_{0.2}O_{19}$ and yet has a smaller expansion suggests that either Ti^{3+} or coupling between the substituents reduces the thermal expansion. Density functional theory calculations of the energies of

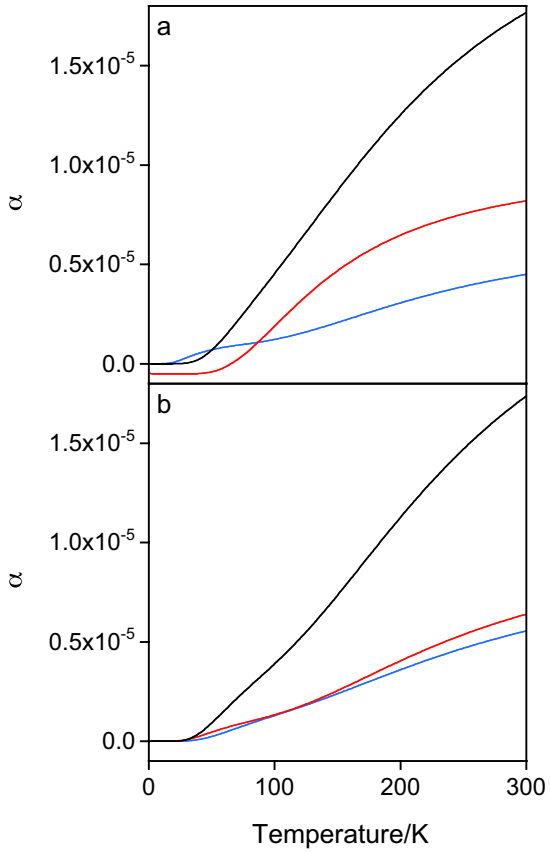

Fig. 5 Temperature dependence of the isobaric thermal expansion coefficients α(*a*) (blue), α(*c*) (red) and α(V) (black) of **a** $CaAl_{11.8}Ti^{3+}_{0.2}O_{19}$, and **b** $CaAl_{9.8}Ti^{3+}_{0.54}Mg_{0.83}Ti.^{4+}_{0.83}O_{19}$

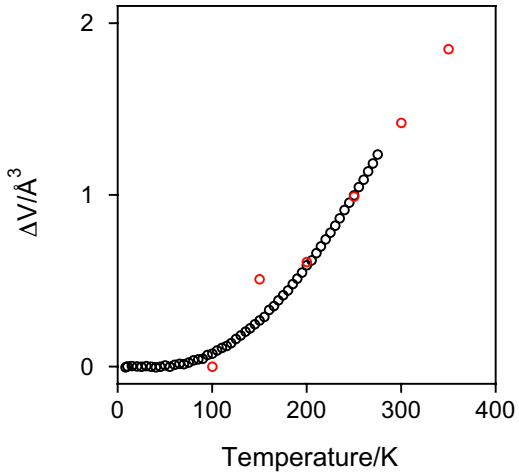

Fig. 6 Change in the unit cell volume of $CaAl_{11.8}Ti^{3+}_{0.2}O_{19}$ (black) and $CaAl_{11}Mg_{0.5}Ti^{4+}_{0.5}O_{19}$ (red; Nagashima et al. 2010) as a function of temperature. Errors are smaller than the size of the symbols

different Ti substitutions in hibonite indicate Ti^{3+}-$Ti^{3+}$and Ti^{4+}-Ti^{4+} interactions across neighbouring sites, while Ti^{3+}-Ti^{4+} interactions may also occur and be associated with a charge transfer transition (Doyle et al. 2014). Indeed, the thermal expansion coefficient α_c for $CaAl_{12}O_{19}$ of 11.8×10^{-6} K^{-1} (Sanchez-Herencia et al. 2000) is larger than that of 11.2×10^{-6} for $CaAl_{11}Mg_{0.5}Ti^{4+}_{0.5}O_{19}$ (Nagashima et al. 2010).

The change in unit cell volume of $CaAl_{11.8}Ti^{3+}_{0.2}O_{19}$ from the present study (10–275 K) is compared to that of a natural sample with the simplified composition $CaAl_{11}Mg_{0.5}Ti^{4+}_{0.5}O_{19}$ (100–923 K; Nagashima et al. 2010) in Fig. 6. The results are in good agreement for the overlapping range despite the differences in Ti oxidation state and site occupancies. Thus, there is little difference in the volume change for Ti^{3+}, Ti^{4+}, or mixed Ti^{3+}-Ti^{4+} hibonites.

Of particular note is the negative thermal expansion of *c* in $CaAl_{11.8}Ti^{3+}_{0.2}O_{19}$ between 10 and 70 K, which balances the positive thermal expansion of *a* to give an effectively constant volume between 10 and 60 K. The fact that the Ti^{3+}-Ti^{4+} sample does not exhibit this behaviour suggests that it may be due to Ti^{3+}, which exclusively occupies the octahedral face-sharing M4 site. The energy of Ti^{3+} occupying adjacent M4 sites (i.e. clustering) was calculated to be 83 $kJmol^{-1}$ more favourable than a random distribution on M4 (Doyle et al. 2014). In other oxides negative thermal expansion has been attributed to rotations of polyhedra linked by bridging oxygens (e.g. Knight 2014; Evans et al. 1998a, b; Welche et al. 1998) that reduce the amount of "free space" in the structure. Such a mechanism is unavailable for face-sharing octahedra. We speculate that the Ti^{3+}-Ti^{3} interaction produces a contraction in the M4 octahedra, which affects the expansion of the R-block. The effect of this contraction is greater than that of the thermal expansion in the absence of Ti^{3+}, resulting in negative thermal expansion, which persists until conventional thermal expansion increases to a point that it dominates.

Supplementary Information The online version contains supplementary material available at https://doi.org/10.1007/s00269-024-01286-5.

Acknowledgements A.J.B. thanks the Engineering and Physical Sciences Research Council (EPSRC) for the award of a CNE Studentship, which was used to support P.M.D. We thank ISIS Neutron Spallation Source for the award of beamtime for proposal RB920090.

Author contributions A.B. wrote the manuscript with contributions from P.S. and P.D. P.D. prepared the samples. All authors were involved with the data acquisition. The data were fit and modelled by P.S., K.K. and P.D.

Funding Open Access funding enabled and organized by CAUL and its Member Institutions.

Data availability No datasets were generated or analysed during the current study.

Declarations

Conflict of interest The authors declare no Conflict of interest.

Open Access This article is licensed under a Creative Commons Attribution 4.0 International License, which permits use, sharing, adaptation, distribution and reproduction in any medium or format, as long as you give appropriate credit to the original author(s) and the source, provide a link to the Creative Commons licence, and indicate if changes were made. The images or other third party material in this article are included in the article's Creative Commons licence, unless indicated otherwise in a credit line to the material. If material is not included in the article's Creative Commons licence and your intended use is not permitted by statutory regulation or exceeds the permitted use, you will need to obtain permission directly from the copyright holder. To view a copy of this licence, visit http://creativecommons.org/licenses/by/4.0/.

References

Beckett JR, Live D, Tsay F-D, Grossman L, Stolper E (1988) Ti^{3+} in meteoritic and synthetic hibonite. Geochim Cosmochim Acta 52:1479–1495

Bermanec VV, Holtstam D, Sturman D, Criddle AJ, Back ME, Scavnicar S (1996) Nezilovite, a new member of the magnetoplumbite group, and the crystal chemistry of magnetoplumbite and hibonite. Can Mineral 34:1287–1297

Berry AJ, Schofield PF, Kravtsova AN, Miller LA, Stephen NR, Walker AM, Soldatov AV, Ireland TR, Geraki K, Mosselmans JFW (2017) The limitations of hibonite as a single-mineral oxybarometer for early solar system processes. Chem Geol 466:32–40

Doyle PM, Schofield PF, Berry AJ, Walker AM, Knight KS (2014) Substitution of Ti^{3+} and Ti^{4+} in hibonite ($CaAl_{12}O_{19}$). Am Miner 99:1369–1382

Doyle PM, Berry AJ, Schofield PF, Mosselmans JFW (2016) The effect of site geometry, Ti content and Ti oxidation state on the Ti K-edge XANES spectrum of synthetic hibonite. Geochim Cosmochim Acta 187:294–310

Evans JSO, Mary TA, Sleight AW (1998a) Negative thermal expansion materials. Physica B 241–243:311–316

Evans JSO, Mary TA, Sleight AW (1998b) Negative thermal expansion in $Sc_2(WO_4)_3$. J Solid State Chem 137:148–160

Giannini M, Boffa Ballaran T, Langenhorst F (2014) Crystal chemistry of synthetic Ti-Mg-bearing hibonites: a single-crystal X-ray study. Am Miner 99:2060–2067

Goodwin AL, Calleja M, Conterio MJ, Dove MT, Evans JSO, Keen DA, Peters L, Tucker MG (2008) Colossal positive and negative thermal expansion in the framework material $Ag_3[Co(CN)_6]$. Science 319:794–797

Hazen RM, Prewitt CT (1977) Effects of temperature and pressure on interatomic distances in oxygen-based minerals. Am Miner 62:309–315

Hernandez-Gomez P, de Francisco C, Brabers VAM, Dalderop JHJ (2000) Thermal expansion of Ti-substituted barium hexaferrite. J Appl Phys 87:3576–3578

Hofmeister AM (2004) Physical properties of calcium aluminates from vibrational spectroscopy. Geochim Cosmochim Acta 68:4721–4726

Hofmeister AM, Wopenka B, Locock AJ (2004) Spectroscopy and structure of hibonite, grossite, and $CaAl_2O_4$: implications for astronomical environments. Geochim Cosmochim Acta 68:4485–4503

Ibberson RM (2009) Design and performance of the new supermirror guide on HRPD at ISIS. Nucl Instrum Methods Phys Res Sect A 600:47–49

Ibberson RM, David WIF, Knight KS (1992) High resolution powder diffractometer (HRPD) at ISIS – a user guide. Report RAL-92-031, 1–25

Ihinger PD, Stolper E (1986) The color of meteoritic hibonite: an indicator of oxygen fugacity. Earth Planet Sci Lett 78:67–79

Knight KS (1996) A neutron powder diffraction determination of the thermal expansion tensor of crocoite ($PbCrO_4$) between 60 K and 290 K. Mineral Mag 60:963–972

Knight KS (2014) The temperature-dependence of the volume expansivity and the thermal expansion tensor of petalite between 4.2 K and 600 K. J Mineral Petrol Sci 109:118–124

Knight KS, Price GD (2008) Powder neutron-diffraction studies of clinopyroxenes. I. The crystal structure and thermoelastic properties of jadeite between 1.5 and 270 K. Can Mineral 46:1593–1622

Knight KS, Stretton IC, Schofield PF (1999) Temperature evolution between 50 K and 320 K of the thermal expansion tensor of gypsum derived from neutron powder diffraction data. Phys Chem Miner 26:477–483

Larson AC, Von Dreele RB (2004) General Structure Analysis System (GSAS). Los Alamos National Laboratory Report LAUR. 86–748

Mary TA, Evans JSO, Vogt T, Sleight AW (1996) Negative thermal expansion from 0.3 to 1050 Kelvin in ZrW_2O_8. Science 272:90–92

Meusburger JM, Hudson-Edwards KA, Tang CC, Connolly E, Crane RA, Fortes AD (2021) Negative linear, in-plane zero and phase-transition-induced negative volume expansion in cranswickite-type $MgSO_4{\cdot}4D_2O$. Acta Crystallogr A77:C1243

Nagashima M, Armbruster T, Hainschwang T (2010) A temperature-dependent structure study of gem-quality hibonite from Myanmar. Mineral Mag 74:871–885

Salomao R, Ferreira VL, de Oliveira IR, Souza ADV, Correr WR (2016) Mechanism of pore generation in calcium hexaluminate (CA_6) ceramics formed in situ from calcined alumina and calcium carbonate aggregates. J Eur Ceram Soc 36:4225–4235

Sanchez-Herencia AJ, Moreno R, Baudin C (2000) Fracture behaviour of alumina-calcium hexaluminate composites obtained by colloidal processing. J Eur Ceram Soc 20:2575–2583

Schofield PF, Knight KS, Stretton IC (1996) Thermal expansion of gypsum investigated by neutron powder diffraction. Am Miner 81:847–851

Schofield PF, Knight KS, Hodson ME, Lanfranco AM (2007) Thermal expansion of deuterated hopeite, $Zn_3(PO_4)_2{\cdot}4D_2O$. Am Miner 92:1038–1047

Toby BH (2001) EXPGUI, a graphical user interface for GSAS. J Appl Crystallogr 34:210–221

Utsunomiya AA, Tanaka K, Morikawa H, Marumo F, Kojima H (1988) Structure refinement of $CaO{\cdot}6Al_2O_3$. J Solid State Chem 75:197–200

Welche PRL, Heine V, Dove MT (1998) Negative thermal expansion in beta-quartz. Phys Chem Miner 26:63–77

Zanetta P-M, Manga VR, Chang Y-J, Ramprasad T, Weber J, Beckett JR, Zega TJ (2023) Atomic-scale characterization of the oxidation state of Ti in meteoritic hibonite: implications for early solar system thermodynamics. Am Miner 108:881–902

Publisher's Note Springer Nature remains neutral with regard to jurisdictional claims in published maps and institutional affiliations.